

Gyrokinetic Simulations of Tokamak Micro-Turbulence Including Kinetic Electron Effects

IDOMURA Yasuhiro, TOKUDA Shinji and KISHIMOTO Yasuaki

*Department of Fusion Plasma Research, Naka Fusion Research Establishment,
Japan Atomic Energy Research Institute, Ibaraki, 311-0193, Japan*

(Received: 9 December 2003 / Accepted: 6 July 2004)

Abstract

A gyrokinetic toroidal particle code for a 3-dimensional nonlinear turbulence simulation (GT3D) has been developed to study the ion temperature gradient driven – trapped electron mode (ITG-TEM) turbulence in tokamak plasmas. From linear zonal flow damping tests and nonlinear ITG simulations, it is shown that a new method based on a canonical Maxwellian distribution is essential to simulate correct zonal flow dynamics in tokamaks. Recently, GT3D has been extended including kinetic trapped electrons. A computational cost of ITG-TEM calculations are drastically reduced by using a new bounce-averaged kinetic trapped electron model. A short wavelength unstable region of the ITG-TEM is calculated using a gyrokinetic field solver with a Pade approximation. From preliminary linear ITG-TEM calculations, the validity of these calculation models are confirmed.

Keywords:

gyrokinetic simulation, ion temperature gradient driven mode, trapped electron mode, electron temperature gradient driven mode

1. Introduction

A global gyrokinetic toroidal particle code for a 3-dimensional nonlinear turbulence simulation (GT3D) [1] has been developed to study the ion temperature gradient driven – trapped electron mode (ITG-TEM) turbulence in tokamak plasmas. The code has been developed based on a finite element particle-in-cell (PIC) method [2], except for several extensions for a nonlinear simulation. Main features of GT3D are summarized as follows. First, we have developed a new method based on a canonical Maxwellian distribution $F_{CM}(P_\varphi, \varepsilon, \mu)$ [1], which is defined by using three constants of motion in the axisymmetric toroidal system, the canonical angular momentum P_φ , the energy ε , and the magnetic moment μ . Second, the conservation property of GT3D is greatly improved using the optimized particle loading [3]. Third, we use a quasi-ballooning representation [4] for nonlinear perturbations, which enables linear and nonlinear global m, n calculations. Fourth, an analysis of the ITG-TEM is enabled by using kinetic trapped electron models. Finally, the code has been optimized for massively parallel scalar and vector machines, and it operates with 40 % and 25 % processing efficiency up to 512 processors respectively on the JAERI Origin3800 system and on the Earth Simulator [5,6].

In this paper, first, we discuss code developments towards the ITG-TEM calculations. A new bounce-averaged kinetic trapped electron model enables order of magnitude low cost

ITG-TEM calculations. A gyrokinetic field solver which can treat a short wavelength unstable region is developed by applying a Pade approximation to the ion polarization density. Linear properties of the ITG-TEM is successfully recovered by using these calculation models. Adding trapped electrons not only increase the growth rate of the ITG mode, but also produce another unstable electron mode, the TEM. Between these two modes, the dominant mode changes depending on k_θ and $\eta_i (= L_n/L_{Ti})$, where k_θ is the poloidal wave number, and L_n and L_{Ti} are scale lengths of density and ion temperature gradients, respectively.

We then discuss zonal flow dynamics in the ITG turbulence. Unlike a conventional method based on a local Maxwellian distribution $F_{LM}(\psi, \varepsilon, \mu)$, which is defined by a flux label ψ , the new F_{CM} method avoids spurious linear driving effect on axisymmetric modes. Through zonal flow damping tests and ITG turbulence simulations, it is found that this spurious driving effect significantly affects zonal flow dynamics and spurious zonal flow oscillations are excited.

The remainder of the paper is organized as follows. In Sec. 2, model equations and numerical methods are described. In Sec. 3, preliminary linear calculations including kinetic trapped electrons are shown and the validity of new models are discussed. In Sec. 4, zonal flow dynamics in the ITG

simulations based on F_{CM} and F_{LM} is discussed. Finally, a summary is given in Sec. 5.

2. Calculation model

2.1 Gyrokinetic equations

The present version of GT3D solves the electrostatic gyrokinetic Vlasov-Maxwell system in a circular concentric tokamak configuration. In the gyro-averaged coordinates, $\mathbf{Z} = (t; \mathbf{R}, v_{\parallel}, \mu, \alpha)$, the electrostatic gyrokinetic Vlasov-Maxwell system [7] is written as

$$\frac{dF_s}{dt} = \frac{\partial F_s}{\partial t} + \frac{d\mathbf{R}}{dt} \cdot \nabla_{\mathbf{R}} F_s + \frac{dv_{\parallel}}{dt} \frac{\partial F_s}{\partial v_{\parallel}} = 0, \quad (1)$$

$$\begin{aligned} \frac{d\mathbf{R}}{dt} &= v_{\parallel} \mathbf{b} + \frac{c}{q_s B_{\parallel}^*} \mathbf{b} \\ &\times \left(q_s \nabla_{\mathbf{R}} \langle \phi \rangle_{\alpha} + m_s v_{\parallel}^2 \mathbf{b} \cdot \nabla_{\mathbf{R}} \mathbf{b} + \mu B \nabla_{\mathbf{R}} \ln B \right), \end{aligned} \quad (2)$$

$$\begin{aligned} \frac{dv_{\parallel}}{dt} &= \\ &- \frac{B^*}{m_s B_{\parallel}^*} \cdot \left(q_s \nabla_{\mathbf{R}} \langle \phi \rangle_{\alpha} + m_s v_{\parallel}^2 \mathbf{b} \cdot \nabla_{\mathbf{R}} \mathbf{b} + \mu B \nabla_{\mathbf{R}} \ln B \right), \end{aligned} \quad (3)$$

$$\begin{aligned} \delta n_s(\mathbf{x}, t) &= \int \delta f_s(\mathbf{R}, v_{\parallel}, \mu, t) \delta([\mathbf{R} + \rho_s] - \mathbf{x}) D_s d^6 \mathbf{Z} \\ &- \frac{n_s q_s}{T_s} \sum_k \left[1 - I_0(k_{\perp}^2 \rho_{ts}^2) \exp(-k_{\perp}^2 \rho_{ts}^2) \right] \phi_k \exp(i\mathbf{k} \cdot \mathbf{x}), \end{aligned} \quad (4)$$

$$-\nabla^2 \phi = 4\pi \sum_s q_s \delta n_s(\mathbf{x}), \quad (5)$$

where \mathbf{R} is a position of the guiding center; $v_{\parallel} = \mathbf{v} \cdot \mathbf{b}$; $v_{\perp} = |\mathbf{v} \times \mathbf{b}|$; $\mu \equiv m_s v_{\perp}^2 / 2B$; $\Omega_s = q_s B / m_s c$; m_s and q_s are the mass and charge of the particle species s , respectively; c is the velocity of light; $\mathbf{b} = \mathbf{B} / B$ is the unit vector in the direction of the magnetic field; α is the gyro-phase angle; $\mathbf{B}^* = \mathbf{B} + (Bv_{\parallel} / \Omega_s) \nabla_{\mathbf{R}} \times \mathbf{b}$; $B_{\parallel}^* = \mathbf{b} \cdot \mathbf{B}^*$; ϕ and ϕ_k are the electrostatic potentials in the configuration and wave number spaces, respectively; $\langle \phi \rangle_{\alpha}$ is the gyro-averaged electrostatic potential; F_0 and δf_s are the equilibrium and perturbed parts of the distribution function F_s , respectively; n_s and δn_s are the equilibrium and perturbed parts of the particle density; T_s is the temperature; D_s is the Jacobian of the gyro-averaged coordinates; I_n is the n -th order modified Bessel function; $k_{\parallel} = \mathbf{k} \cdot \mathbf{b}$ and $k_{\perp} = |\mathbf{k} \times \mathbf{b}|$ are the parallel and perpendicular component of the wave vector \mathbf{k} and ρ_{ts} is the Larmor radius evaluated with the thermal velocity v_{ts} .

2.2 Trapped electron models

In principle, kinetic electrons can be described by taking a drift-kinetic limit of the gyrokinetic equation, Eqs. (1)–(3). In the present study, we have developed two drift-kinetic electron models. One is a full drift-kinetic electron model and the other is a drift-kinetic trapped electron model with adiabatic passing electrons. From linear benchmark tests, we have confirmed that both models give the almost same frequency

and growth rate spectra of the ITG-TEM. This means that passing electrons respond almost adiabatically to the ITG-TEM with $\omega / k_{\parallel} \ll v_{te}$, where ω is the frequency of the ITG-TEM. Since the high frequency ω_H mode [8] does not appear in the latter model, the computational cost of the latter model is order of magnitude lower than the former model. However, the computational cost of the drift-kinetic trapped electron model is still high, because the Courant-Friedrichs-Lewy (CFL) condition is limited by the electron bounce frequency ω_{be} , and the ballistic noise is inevitable in the drift-kinetic model. In order to resolve these problems, we have developed a bounce-averaged kinetic electron model based on the bounce-averaged kinetic equation [9]. In the bounce-averaged kinetic formalism, the fast bounce motion is eliminated by applying the Lie perturbation theory under the ordering, $\omega / \omega_{be} \sim \mathcal{O}(\epsilon)$. In the deeply trapped approximation, $\kappa^2 \ll 1$, the bounce-averaged coordinates $(\beta_b, \alpha_b, \Psi, I, \mu, \alpha)$ are given as

$$\beta_b \equiv \Psi, \quad (6)$$

$$\alpha_b \equiv \varphi - q\theta, \quad (7)$$

$$\Psi = \pi + \text{sgn}(v_{\parallel}) \left[\arcsin \left(\frac{\sin(\theta/2)}{\kappa} \right) + \frac{\pi}{2} \right], \quad (8)$$

$$I = 2qR_0 \sqrt{m_s \varepsilon_r \mu \bar{B} \kappa^2}, \quad (9)$$

where θ and φ are the poloidal and toroidal angle, respectively, q is the safety factor, κ is the pitch angle, R_0 is the major radius, $\varepsilon_r = r/R_0$, and \bar{B} is a flux surface averaged magnetic field. In this coordinates, the bounce-averaged Hamiltonian H_0 and the corresponding kinetic equation are obtained as,

$$H_0(\beta_b, I, \mu) = \mu \bar{B} (1 - \varepsilon_r) + \frac{1}{qR_0} \sqrt{\frac{\varepsilon_r \mu \bar{B}}{m_s}} I, \quad (10)$$

$$\frac{dF_b}{dt} = \frac{\partial F_b}{\partial t} + \frac{d\beta_b}{dt} \frac{\partial F_b}{\partial \beta_b} + \frac{d\alpha_b}{dt} \frac{\partial F_b}{\partial \alpha_b} = 0, \quad (11)$$

$$\frac{d\beta_b}{dt} = c \frac{\partial \langle \phi \rangle_{\Psi}}{\partial \alpha_b}, \quad (12)$$

$$\frac{d\alpha_b}{dt} = -\frac{c}{q_s} \frac{\partial H_0}{\partial \beta_b} - c \frac{\partial \langle \phi \rangle_{\Psi}}{\partial \beta_b}, \quad (13)$$

where $\langle \phi \rangle_{\Psi}$ is the bounce-averaged electrostatic potential. Since the action integral I is an exact invariant in the bounce-averaged coordinates, the Hamiltonian H_0 does not depend on the corresponding conjugate variable Ψ , and the fast bounce motion and the associated ballistic noise are eliminated from the equation system. Accordingly, the CFL condition of the bounce-averaged kinetic electron model is almost comparable with that of ITG calculations, and the numerical convergence against the number of bounce centers

is drastically improved compared with the drift-kinetic electron model. In the electron (zero banana width) limit, the trapped particle density is given as

$$\delta n_b(\psi, \theta, \varphi) = \int \delta f_b(\beta_b(\psi), \alpha_b(\psi, \theta, \varphi), I', \mu') \delta(\Psi' - \Psi(\psi, \theta, \varphi, I')) D_b d\Psi' dI' d\mu' d\alpha'. \quad (14)$$

The bounce-average in Eqs. (12), (13) and (14) is calculated using a finite sampling point average along the bounce orbit whose turning points are determined by I or the pitch angle κ of each particles. Actually, 20 ~ 80 sampling points are chosen along the field line by following $\Delta\theta = v_{\parallel}/qR_0\Delta t$ with a constant Δt .

Another extension of the code for TEM calculations is a treatment of the ion polarization density. When we consider the ITG turbulence with adiabatic electrons, where a linear unstable region is limited for $k_{\theta}\rho_{ii} < 0.6$ (see Fig. 3), a Taylor expansion for the ion polarization density (the second term in Eq. (4)), $1 - I_0(b)e^{-b} \sim b$, is a relatively good approximation. Under a long wavelength approximation, $k_{\perp}^2\rho_{ii}^2 \ll 1$, Eqs. (4) and (5) yield the gyrokinetic Poisson equation for the ITG mode,

$$\begin{aligned} & -\nabla_{\perp} \cdot \frac{\rho_{ii}^2}{\lambda_{Di}^2} \nabla_{\perp} \phi + \frac{1}{\lambda_{De}^2} (\phi - \langle \phi \rangle_{\theta}) \\ & = 4\pi q_i \int \delta f_i(\mathbf{R}, v_{\parallel}, \mu, t) \delta([\mathbf{R} + \rho_i] - \mathbf{x}) D_i d^6\mathbf{Z}, \end{aligned} \quad (15)$$

where $\langle \phi \rangle_{\theta}$ is the flux surface averaged potential and λ_{Ds} is the Debye length. On the other hand, in analyzing the ITG-TEM turbulence, which has a broad unstable spectrum up to a short wavelength region or $k_{\theta}\rho_{ii} \sim 0.6$, we use a Pade approximation for the ion polarization density, $1 - I_0(b)e^{-b} \sim b/(1+b)$ [10]. By using a Pade approximation, the gyrokinetic field equation for the ITG-TEM turbulence is obtained as,

$$\begin{aligned} & -\nabla_{\perp} \cdot \frac{\rho_{ii}^2}{\lambda_{Di}^2} \nabla_{\perp} \phi + (1 + \nabla_{\perp} \cdot \rho_{ii}^2 \nabla_{\perp}) \frac{c_p}{\lambda_{De}^2} (\phi - \langle \phi \rangle_{\theta}) \\ & = 4\pi(1 + \nabla_{\perp} \cdot \rho_{ii}^2 \nabla_{\perp}) \left[q_i \int \delta f_i \delta([\mathbf{R} + \rho_i] - \mathbf{x}) D_i d^6\mathbf{Z} + q_e \delta n_t \right], \end{aligned} \quad (16)$$

where c_p is a fraction of passing electrons and δn_t is the trapped particle density. In the code, the gyrokinetic field equation is solved using a finite element method [11] with a fixed boundary condition $\phi = 0$ at $r = a$ and a natural boundary condition at $r = 0$.

2.3 New δf method based on canonical Maxwellian

In a nonlinear characteristic δf method [12], δf , which is defined as a deviation from F_0 , is solved numerically using a nonlinear characteristic method. In this method, an evolution equation of δf along nonlinear characteristics or perturbed particle orbits is described by

$$\frac{d\delta f}{dt} = - \left[\frac{d\mathbf{R}}{dt} \Big|_1 \cdot \nabla_{\mathbf{R}} F_0 + \frac{dv_{\parallel}}{dt} \Big|_1 \frac{\partial F_0}{\partial v_{\parallel}} \right], \quad (17)$$

where $d\mathbf{R}/dt|_1$ and $dv_{\parallel}/dt|_1$ show the perturbed part of non-linear characteristics. Eq. (17) is valid when F_0 is an equilibrium solution, which satisfies $dF_0/dt = 0$. In the axisymmetric toroidal system, an exact equilibrium solution is given by a canonical Maxwellian distribution, $F_{CM}(P_{\varphi}, \varepsilon, \mu)$. However, the conventional δf method was developed based on a local Maxwellian distribution, $F_{LM}(\psi, \varepsilon, \mu)$. Since ψ is not a constant of motion in the axisymmetric toroidal system, F_{LM} does not satisfy $dF_0/dt = 0$. In the conventional δf method, Eq. (17) has been used by ignoring a variation of F_{LM} along the unperturbed characteristics, $d\mathbf{R}/dt|_0 \cdot \nabla_{\mathbf{R}} F_{LM} + dv_{\parallel}/dt|_0 \partial v_{\parallel} F_{LM}$. Obviously, this treatment violates the conservation property of the gyrokinetic equation. In a new δf method, we use F_{CM} in calculating the r.h.s. of Eq. (17). In the flux coordinates $(\psi, \theta, \varphi, v_{\parallel}, \mu, \alpha)$, Eq. (17) is written as

$$\begin{aligned} \frac{d\delta f}{dt} = & - \left[\frac{d\mathbf{R}}{dt} \Big|_1 \cdot \left(\frac{\partial \psi_C}{\partial \psi} \nabla \psi + \frac{\partial \psi_C}{\partial \theta} \nabla \theta \right) \frac{\partial F_{CM}}{\partial \psi_C} \right. \\ & \left. + \frac{dv_{\parallel}}{dt} \Big|_1 \left(\frac{\partial \psi_C}{\partial v_{\parallel}} \frac{\partial F_{CM}}{\partial \psi_C} + \frac{\partial F_{CM}}{\partial v_{\parallel}} \right) \right], \end{aligned} \quad (18)$$

where $\psi_C = -(c/q_s)P_{\varphi}(\psi, \theta, v_{\parallel})$. Since the new method is constructed straightforwardly based on F_{CM} , it keeps the conservation property of the system.

3. Linear ITG-TEM calculations

Simulations have been performed using Cyclone base case parameters [13]: deuterium plasma, $R_0 = 1.3$ m, $a = 0.48$ m ~ $150\rho_{ii}$, $B_0 = 1.9$ T, $T_e = T_i$, $R_0/L_{ii} = 6.92$, $R_0/L_n = 2.22$ at a reference surface or $r_0 = 0.5a$. The q profile is given as $q = 0.84 + 2.18(r/a)^2$ ($q(r_0) = 1.4$, $s(r_0) = 0.776$).

Figure 1 shows the η_i dependence of the growth rate and frequency. In the frequency spectrum, it is shown that the ITG-TEM has two independent branches, the ITG mode and the TEM, which propagate in the ion and electron diamagnetic directions, respectively [14]. In the adiabatic electron case, a critical η_i exists near $\eta_i \sim 2$. On the other hand, in the kinetic electron case, a critical η_i disappears, and the ITG-TEM is destabilized by trapped electrons even at $\eta_i = 0$ [15]. In a transition region near $\eta_i \sim 2.5$, both the ITG mode and the TEM coexist. In the figure, the bounce-averaged kinetic electron case shows reasonably good agreement with the drift-kinetic trapped electron case. Differences of the real frequency (~ 20 %) and the growth rate (~ 10 %) in a low η_i region, where the TEM becomes dominant, may be due to a deeply trapped assumption $\kappa^2 \ll 1$ or a large aspect ratio assumption $r/R_0 \ll 1$ used in the present bounce-average formalism.

Figure 2 shows the k_{θ} spectrum of the ITG-TEM. As in the adiabatic electron case (see Fig. 3), the growth rate spectrum of the ITG mode peaks at $k_{\theta}\rho_{ii} \sim 0.3$, but the growth

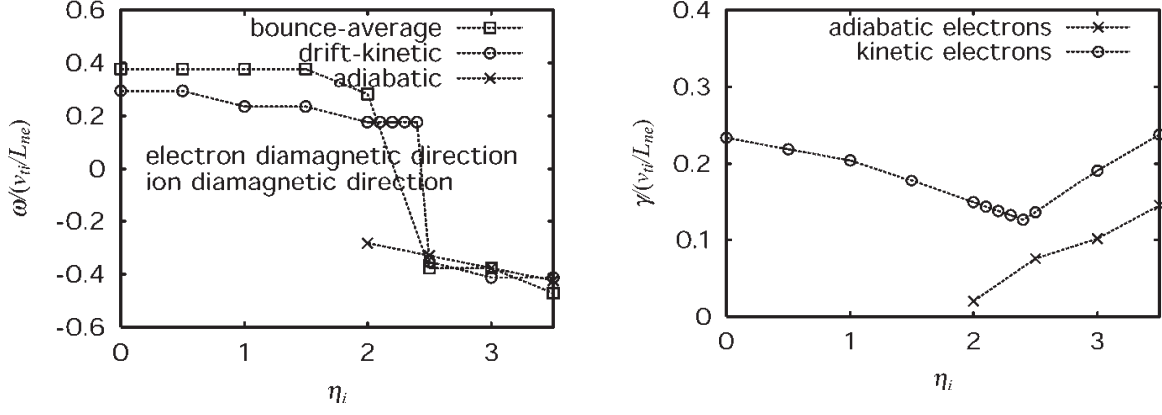


Fig. 1 The η_i dependences of growth rate and frequency are plotted for the ITG-TEM (drift-kinetic trapped electrons: open circle, bounce-averaged kinetic trapped electrons: open square) and the ITG mode (adiabatic electrons: cross) in Cyclone base case plasmas $k_\theta \rho_{ii} = 0.275$.

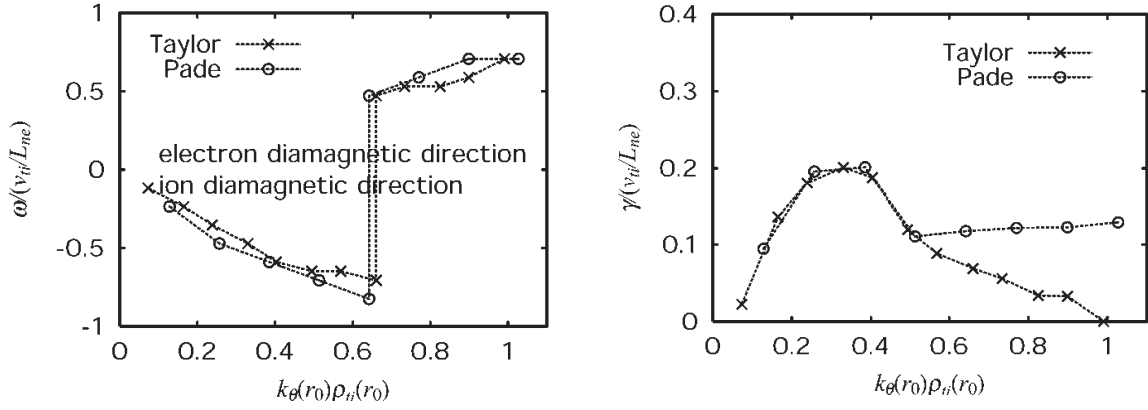


Fig. 2 The growth rate and frequency spectra of the ITG-TEM in Cyclone base case plasmas ($R_0/L_{ii} = 6.92$, $\eta_i = 3.12$). Results obtained from gyrokinetic Poisson field solvers with a long wavelength approximation (Taylor) and with a Pade approximation are compared.

rate itself is enhanced by trapped electrons which do not respond to the ITG mode adiabatically. In a high k_θ region, the ITG mode is stabilized by the finite Larmor radius (FLR) effect, and the TEM becomes dominant. This high k_θ region with $k_\theta \rho_{ii} > 0.6$ can not be analyzed by using a gyrokinetic Poisson equation with a long wavelength approximation, $(k_\theta \rho_{ii})^2 \ll 1$. On the other hand, a gyrokinetic field solver with a Pade approximation successfully captures the high k_θ ITG-TEM. It is noted that a linear ITG-TEM benchmark among GT3D, GTC (a global gyrokinetic PIC code), and FULL (a local gyrokinetic ballooning code) is now going on, and these three codes show reasonably good agreements for the linear frequency and growth rate spectra [16].

4. Zonal flow dynamics in plasmas with canonical Maxwellian distribution

In most of conventional gyrokinetic simulations, a local Maxwellian distribution $F_{LM}(\psi, \varepsilon, \mu)$ has been used as an approximate equilibrium solution. Besides the problem related to the conservation property of the δf scheme, a gyrokinetic simulation based on F_{LM} has the following problem. According to the linear gyrokinetic equation in the canonical coordinates, $(P_\varphi, \theta, \varphi, \varepsilon, \mu, \alpha)$ [17],

$$\frac{d}{dt} \Big|_0 \delta f = q \frac{\partial \langle \phi \rangle_\alpha}{\partial \varphi} \frac{\partial F_{CM}}{\partial P_\varphi} - q \frac{\partial \langle \phi \rangle_\alpha}{\partial t} \frac{\partial F_{CM}}{\partial \varepsilon}, \quad (19)$$

there is no linear driving effect on axisymmetric modes, because the driving term associated with $\partial F_{CM} / \partial P_\varphi$ (the pressure gradient in the P_φ direction) disappears. It is noted that in the zero orbit width limit, the P_φ direction becomes the radial direction or the ψ direction. But, if we replace $F_{CM}(P_\varphi, \varepsilon, \mu)$ by $F_{LM}(\psi(P_\varphi, \theta, \varepsilon), \varepsilon, \mu)$, we have

$$\frac{d}{dt} \Big|_0 \delta f = \left[q \frac{\partial \langle \phi \rangle_\alpha}{\partial \varphi} \frac{\partial \psi}{\partial P_\varphi} - q \frac{\partial \langle \phi \rangle_\alpha}{\partial t} \frac{\partial \psi}{\partial \varepsilon} \right] \frac{\partial F_{LM}}{\partial \psi} - q \frac{\partial \langle \phi \rangle_\alpha}{\partial t} \frac{\partial F_{LM}}{\partial \varepsilon}. \quad (20)$$

In a F_{LM} model, the driving term associated with $\partial F_{LM} / \partial \psi$ (the radial pressure gradient) can drive axisymmetric modes through the second term in Eq. (20). For finite toroidal mode number ($n \neq 0$) modes, this spurious driving effect is just a higher order minor correction compared with the dominant driving effect in the first term, and the linear theory of micro-

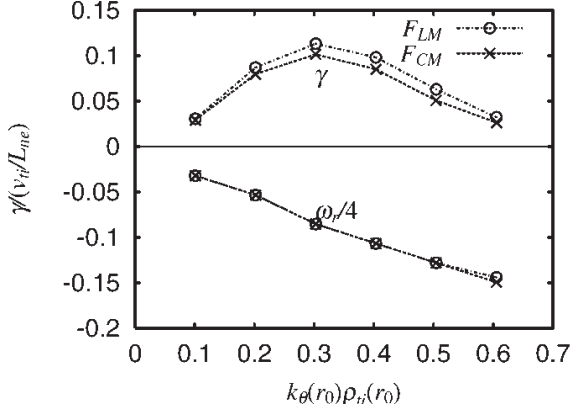


Fig. 3 The eigenfrequency spectra of the ITG mode with adiabatic electrons are calculated for Cyclone base case plasmas with F_{CM} and F_{LM} .

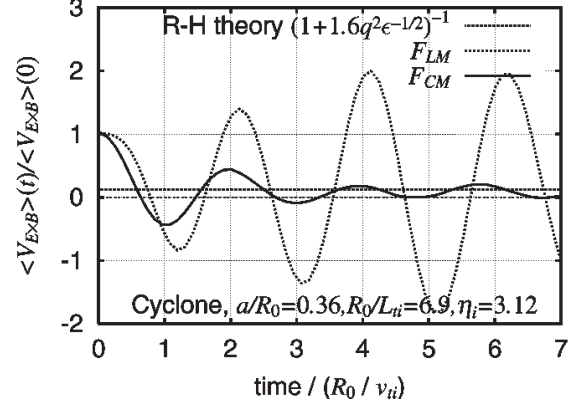


Fig. 4 Zonal flow damping tests in Cyclone base case plasmas with F_{CM} and F_{LM} . In the F_{CM} case, the residual flow level agrees well with the theory.

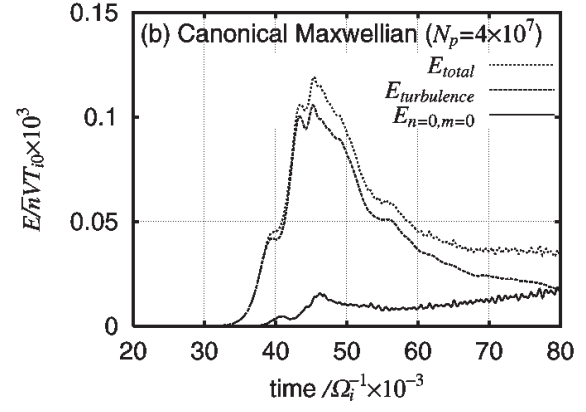
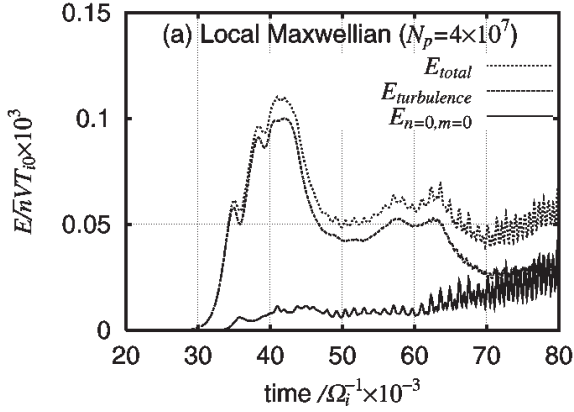


Fig. 5 The fluctuation field energy in ITG turbulence simulations with F_{CM} and F_{LM} . Cyclone base case plasmas are simulated with $N_p = 4 \times 10^7$ marker particles. $E_{turbulence}$ and $E_{n=0,m=0}$ show the turbulent and zonal flow components, respectively ($E_{total} = E_{turbulence} + E_{n=0,m=0}$). In the nonlinear phase, spurious zonal flow oscillations grow in the F_{LM} case.

instabilities has been developed successfully based on a F_{LM} model. However, for the axisymmetric perturbations, where the dominant driving term disappears, the spurious driving term may be more significant.

In order to examine these points, we have performed linear calculations of the ITG mode and zonal flow damping tests [18] in Cyclone base case plasmas with F_{CM} and F_{LM} . In Fig. 3, both the F_{CM} and F_{LM} cases give similar growth rate and frequency spectra, and both results agree well with the previous linear benchmark calculations [13]. On the other hand, in zonal flow damping tests (see Fig. 4), the F_{CM} and F_{LM} cases show quite different behaviors. In the F_{CM} case, zonal flows are damped rapidly with $m = 1$ damping oscillations and the residual zonal flow level agrees well with the theoretical prediction [18]. However, in the F_{LM} case, spurious zonal flow oscillations are excited. This result is inconsistent with the linear gyrokinetic theory, which predicts no driving effect on axisymmetric perturbations including zonal flows.

Figure 5 shows the time history of the fluctuation field energy in ITG turbulence simulations. In the F_{LM} case, zonal flow oscillations grow after the nonlinear saturation. On the

other hand, in the F_{CM} case, the zonal flow energy keeps a quasi-steady state. These zonal flow oscillations are often discussed as the geodesic acoustic mode (GAM). Since zonal flows are linearly stable, some nonlinear turbulent drive is needed to excite GAM. However, according to the saturation amplitude and the turbulent spectra in the initial saturation phase, such a nonlinear driving effect is expected to be almost the same in both cases. Thus, it is considered that zonal flow oscillations are excited by a spurious linear driving effect on zonal flows in plasmas with F_{LM} .

5. Summary

Through zonal flow damping tests and ITG simulations, a spurious driving effect of F_{LM} on zonal flows are identified. This result shows an importance of a new F_{CM} model in gyrokinetic turbulence simulations where zonal flows play a significant role. For the ITG-TEM calculations, GT3D is extended including kinetic trapped electrons. A computational cost of ITG-TEM calculations is drastically reduced by a newly developed bounce-averaged kinetic trapped electron model. A short wavelength unstable region of the ITG-TEM

is successfully calculated using a gyrokinetic field solver with a Pade approximation. The validity of these models are confirmed through the preliminary linear ITG-TEM calculations. The results show that trapped electrons drastically change ion-scale micro-instabilities. The ITG-TEM turbulence simulation is essential for a comprehensive study of the anomalous ion/electron heat transport and the anomalous particle transport. In a future work, nonlinear ITG-TEM simulations will be addressed.

Acknowledgments

One of the authors (Y.I.) would like to acknowledge G. Rewoldt, Z. Lin, A. Bottino, and T.S. Hahm for their useful discussions on ITG-TEM calculations. The authors thank M. Kikuchi, H. Ninomiya, and W.M. Tang for their support. The simulations were performed on the JAERI Origin3800 system.

References

- [1] Y. Idomura, S. Tokuda and Y. Kishimoto, Nucl. Fusion **43**, 234 (2003).
- [2] M. Fivaz, S. Brunner, G. Ridder *et al.*, Comput. Phys. Commun. **111**, 27 (1998).
- [3] R. Hatzky, T.M. Tran, A. Könies *et al.*, Phys. Plasmas **9**, 898 (2002).
- [4] R. Gruber, S. Semenzato, F. Troyon *et al.*, Comput. Phys. Commun. **24**, 363 (1981).
- [5] Y. Idomura, M. Adachi, K. Gorai *et al.*, J. Plasma Fusion Res. **79**, 172 (2003).
- [6] Y. Kishimoto, Annual Report of the Earth Simulator Center April 2002 – March 2003, 201 (2003).
- [7] T.S. Hahm, Phys. Fluids **31**, 2670 (1988).
- [8] W.W. Lee, J. Comput. Phys. **72**, 243 (1987).
- [9] B.H. Fong and T.S. Hahm, Phys. Plasmas **6**, 188 (1999).
- [10] G. Hammett, W. Dorland and F.W. Perkins, Phys. Fluids B **4**, 2052 (1992).
- [11] A. Bottino, T.M. Tran, O. Sauter *et al.*, *Theory of Fusion Plasmas*, Int. Workshop, (2001).
- [12] S.E. Parker and W.W. Lee, Phys. Fluids B **5**, 77 (1993).
- [13] A.M. Dimits, G. Bateman, M.A. Beer *et al.*, Phys. Plasmas **7**, 969 (2000).
- [14] J.Q. Dong, S.M. Mahajan and W. Horton, Phys. Plasmas **4**, 755 (1997).
- [15] G. Rewoldt and W.M. Tang, Phys. Fluids B **2**, 318 (1990).
- [16] G. Rewoldt, Z. Lin and Y. Idomura, Bull. Am. Phys. Soc. **48**, 219 (2003).
- [17] S. Wang, Phys. Rev. E **64**, 056404 (2001).
- [18] M.N. Rosenbluth and F.L. Hinton, Phys. Rev. Lett. **80**, 724 (1998).